

Orthogonal Electric Control of the Out-Of-Plane Field-Effect in 2D Ferroelectric α - In_2Se_3

Yue Li, Chen Chen, Wei Li, Xiaoyu Mao, Heng Liu, Jianyong Xiang, Anmin Nie, Zhongyuan Liu, Wenguang Zhu,* and Hualing Zeng*

Tuning the electric properties of crystalline solids is at the heart of material science and electronics. Generating the electric field-effect via an external voltage is a clean, continuous, and systematic method. Here, utilizing the unique electric dipole locking in van der Waals (vdW) ferroelectric α - In_2Se_3 , a new approach is reported to establish the electric gating effect, where the electrostatic doping in the out-of-plane direction is induced and controlled by an in-plane voltage. With the vertical vdW heterostructure of ultrathin α - In_2Se_3 and MoS_2 , an in-plane voltage gated coplanar field-effect transistor with distinguished and retentive on/off ratio is validated. The results demonstrate unprecedented electric control of ferroelectricity, which paves the way for integrating 2D ferroelectric into novel nanoelectronic devices with broad applications.

Field effect, the ability of electrically modulating carrier density in solid material, is not only the fundamental of semiconductor based information technology, but also crucial for studying a wide variety of field-induced rich phenomena in fundamental science, such as unconventional superconductivity,^[1–3] exotic magnetism,^[4] emergent phase transition,^[5–7] and topological quantum transport.^[8,9] To generate electric gating, the universal

scheme is constructing the device referred to as field-effect transistor (FET), in which an external voltage can be applied to vary the carrier doping of the material in the conducting channel. To date, there have been delivered several types of FETs.^[5,7,10–14] Subject to specific gate dielectric, the FETs function in distinctive way, including electrostatically accumulation of carriers via oxide insulator or ferroelectrics,^[12–14] forming the electric double layer of large capacitance by organic ionic liquids,^[10,11,15] and driving ion intercalation from recently developed solid ionic gel or conductor.^[5,7] However, limited by the linear electric response of conventional


gate dielectrics, the device geometry in most field-effect studies is fixed to be capacitor-like by placing an indispensable gate electrode either on top or at bottom to sandwich the dielectrics. The field-effect is therefore induced by the gate electric field, which is always perpendicular to the conducting channel. This stereo structure geometry consequently increases the device complexity and furtherly limits its application in specific areas only. To that end, FETs with new conceptual design is highly desired, especially for developing flexible nanoelectronics and optoelectronics with van der Waals (vdW) materials.

In this work, to overcome the limitation, we present a new approach to create a vertical field-effect in a coplanar device with layered α - In_2Se_3 as the gate dielectric. α - In_2Se_3 is an emerging 2D ferroelectric semiconductor with remarkable optical and transport properties.^[16–19] Recent studies have confirmed its stable room-temperature ferroelectricity at the single atomic layer limit with the unique intercorrelation of out-of-plane and in-plane electric polarizations.^[20–26] For ferroelectrics, especially when forming heterostructures, their polarity is an effective knob to tune the electrostatic doping as well as the global electronic structure, resulting practical device potential such as ferroelectric field-effect transistors (FeFETs).^[27] This same scenario is applicable to all 2D ferroelectrics with OOP electric polarizations.^[13,28,29] In addition to the OOP ferroelectricity, α - In_2Se_3 presents the unique inter-locking feature of electric dipoles. The flipping of the IP electric polarization in α - In_2Se_3 can be achieved by an OOP bias,^[21,24] or vice versa. Therefore, it suggests that one can develop coplanar FET (CP-FET) with ultrathin α - In_2Se_3 , where the out-of-plane (OOP) electric gating effect is controlled by an in-plane (IP) voltage.

Our results are summarized in the following. We verify that the IP and OOP electric polarization in 3R α - In_2Se_3 thin

Y. Li, C. Chen, X. Mao, H. Liu, Prof. W. Zhu, Prof. H. Zeng
 International Center for Quantum Design of Functional
 Materials (ICQD)
 Hefei National Laboratory for Physical Science at the Microscale
 and Synergetic Innovation Center of Quantum Information and
 Quantum Physics
 University of Science and Technology of China
 Hefei, Anhui 230026, China
 E-mail: wgzhu@ustc.edu.cn; hlzeng@ustc.edu.cn

Y. Li, C. Chen, W. Li, X. Mao, H. Liu, Prof. W. Zhu, Prof. H. Zeng
 Key Laboratory of Strongly-Coupled Quantum Matter Physics
 Chinese Academy of Sciences
 Department of Physics
 University of Science and Technology of China
 Hefei, Anhui 230026, China
 Prof. J. Xiang, Prof. A. Nie, Prof. Z. Liu
 State Key Laboratory of Metastable Materials Science and Technology
 Yanshan University
 Qinhuangdao 066004, China

 The ORCID identification number(s) for the author(s) of this article can be found under <https://doi.org/10.1002/aelm.202000061>.

© 2020 The Authors. Published by WILEY-VCH Verlag GmbH & Co. KGaA, Weinheim. This is an open access article under the terms of the Creative Commons Attribution License, which permits use, distribution and reproduction in any medium, provided the original work is properly cited.

DOI: 10.1002/aelm.202000061

layers are inherently coupled, which is consistent with previous studies.^[20,21,24] Such correlation is observed in both spontaneous and artificial ferroelectric domains. Based on the electric dipole locking, we experimentally show the reversible switch of the OOP electric polarization via the bias in a two-electrode planar device of layered α -In₂Se₃ only. In particular, we find large surface potential difference (≈ 100 mV) for oppositely polarized ferroelectric domains. This can be well understood as a result of the accumulated negative or positive polarization charges on the domain surface. We fabricate the CP-FET by stacking the vertical vdW heterostructure with ultrathin MoS₂ and α -In₂Se₃. In the device, the conductance of few layer MoS₂ can be reversibly tuned by the in-plane polarizing voltage applied on α -In₂Se₃. With the nonvolatile nature of ferroelectrics, the as-prepared CP-FET functions with distinguished and retentive on/off ratio. The findings in this work demonstrate a new way of manipulating ferroelectricity, which enables the unprecedented function control with simple device architecture.

Figure 1 depicts the schematic lattice structure of α -In₂Se₃ and the corresponding ferroelectricity. Bulk α -In₂Se₃ holds

rhombohedral $R3m$ layered crystal structure (Figure 1a). Inside the unit cell, there are three quintuple layers (QLs), which contains five covalently bonded atomic layers in the sequence of Se–In–Se–In–Se. In each α -In₂Se₃ QL, the central Se atoms are asymmetrically bonded to four In atoms, forming tetrahedron structure. Consequently, the interlayer spacings between the middle Se layer and its neighboring two In layers are dramatically different. This subtle atomic configuration of the central Se atoms leads to the emergence of ferroelectricity in α -In₂Se₃. As the shown in Figure 1b, by projecting all the atoms of a given QL onto c axis and a axis (or b axis), it is clear to find that the spatial inversion symmetry is explicitly broken along both IP and OOP directions. The deviation of the middle Se atom from the inversion center contributes to the generation of net electric dipole in the OOP direction as well as in the IP direction. With 180° in plane rotation of the QL, while remaining the lattice structure and symmetry unchanged, the IP and OOP electric polarizations are reversed, establishing the degenerate ferroelectric states in each direction. Most importantly, the crystal lattice of α -In₂Se₃ guarantees the intercorrelation between the

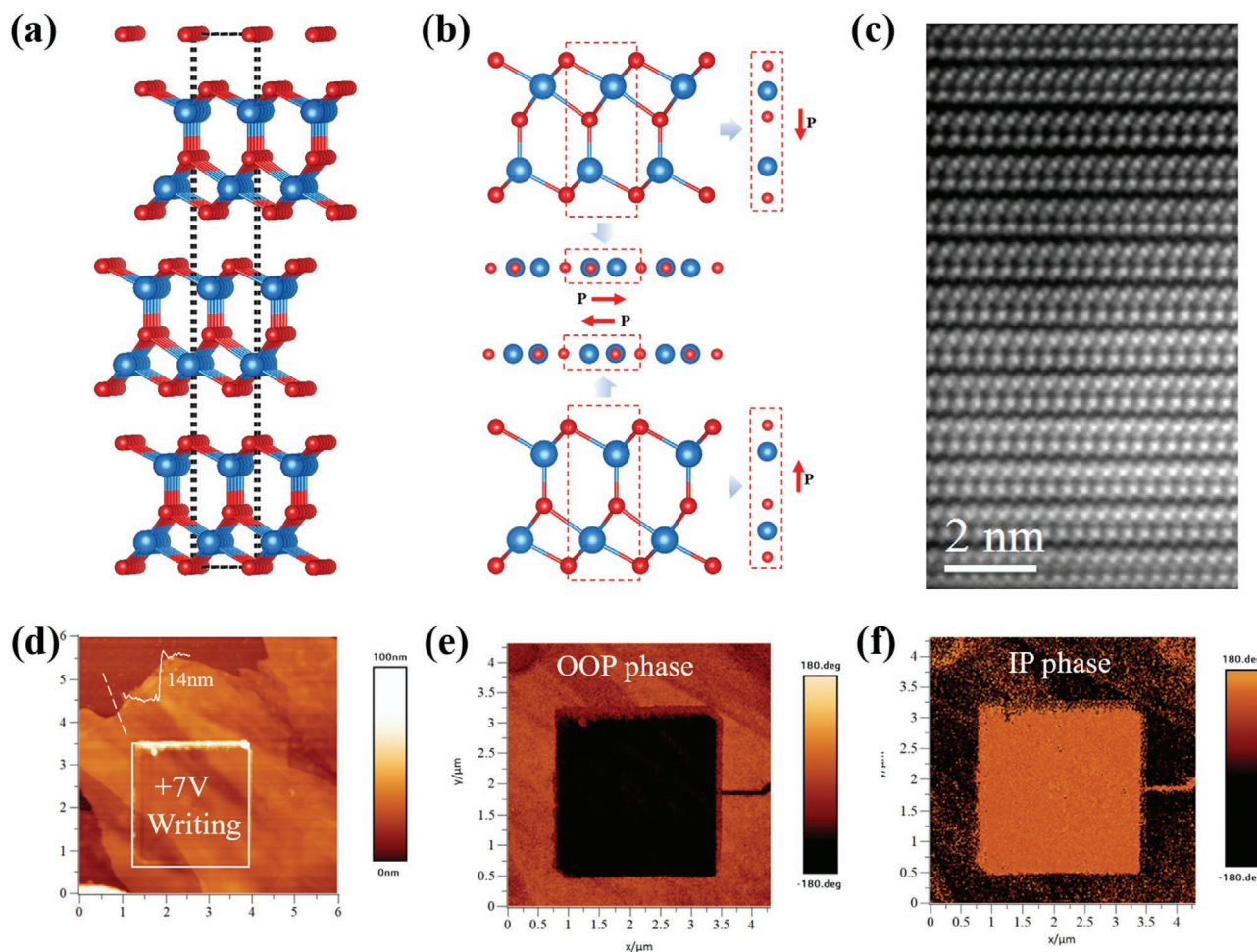


Figure 1. Ferroelectric polarization locking in α -In₂Se₃. a) Crystal structure of 3R α -In₂Se₃. Indium atoms and Selenium atoms are presented in blue and red respectively. b) Side views of the two oppositely polarized states of one QL α -In₂Se₃. Projection of the atoms into c and a (or b) axis indicated the spontaneously intercorrelated electric polarizations in α -In₂Se₃. The directions of the electric polarization were indicated by red arrows. c) Cross-sectional high-resolution STEM image of an α -In₂Se₃ nanoflake. Scale bar: 2 nm. d) Topography and e, f) PFM measurements of 14 nm thick α -In₂Se₃. The ferroelectric domains in the OOP and IP directions are correlated.

IP and OOP electric polarizations, which makes it possible to manipulate the electric polarization in one direction by controlling the other. This is the unique feature of 2D α -In₂Se₃ that is absent in intensively studied ferroelectrics, such as perovskite oxides BaTiO₃, the organic poly(vinylidene fluoride-co-trifluoroethylene) (PVDF-TrFE) thin film and recently discovered 2D CuInP₂S₆.

The α -In₂Se₃ flakes studied here were mechanically exfoliated from bulk crystals (details can be found in the Experimental Section). To confirm its crystalline structure, we characterized our samples with aberration-corrected scanning transmission electron microscopy (AC-STEM) and the Raman technique. Figure 1c shows a typical high-resolution STEM image. From this atomically resolved cross sectional view, the α -In₂Se₃ thin layer is found to be truly following the 3R stacking order with each unit cell contained three shifted QLs, which is identical with the schematic atom model as displayed in Figure 1a. In addition, we performed the Raman scattering measurements to show the sample uniformity and quality at macroscopic scale. Phonon modes centered at 90, 104, 182, 201, and 251 cm⁻¹ were observed in the Raman spectrum of typical samples (Figure S1, Supporting Information). The red shift of A₁ vibration mode to 104 cm⁻¹ indicates the phonon softening in the ferroelectric phase. All these phonon modes are in good agreement with the results from previous studies on ferroelectric 3R α -In₂Se₃.^[21,22,26,29] The Raman features, together with the AC-STEM results, exclusively confirm the 3R crystal structure nature of α -In₂Se₃ thin layers studied in this work.

As the first step, we verified the ferroelectric polarization coupling in α -In₂Se₃ via the piezo force microscopy (PFM). The α -In₂Se₃ nanoflakes were post transferred onto conductive Au/SiO₂ substrate (details can be found in the Experimental Section). As shown in Figure S3 (Supporting Information), the IP and OOP spontaneous ferroelectric domains are clearly visualized in the PFM phase images of α -In₂Se₃ few layers. The phase contrast between adjacent domains is observed to be 180°, indicating the antiparallel ordering of the electric dipoles in both the two directions. By comparing the IP and OOP PFM phase images, we found almost identical distribution of the ferroelectric domains. This strong correlation can be regarded as one evidence of the electric dipole inter-locking in α -In₂Se₃. However, when the polar axis of the studied ferroelectric is not strictly parallel or perpendicular to the PFM tip, same domain patterns will be produced in the IP and OOP directions as a result of the electric dipole projection. Therefore, to exclude such mechanism, we tested the simultaneous switching of the electric polarization in ferroelectric α -In₂Se₃ by an OOP electric field. Figures 1d–f presents a square artificial ferroelectric domain established by +7 V vertical bias on one 14 nm thick sample. The surface topography measured after the writing process indicates that there is no damage to the sample under this bias. The flip of the OOP electric polarization is intuitively indicated by the strong phase contrast in the electrically written area as shown in Figure 1e. At the same time, we observed corresponding IP phase change in the same region (Figure 1f), indicating the concurrent switch of IP electric dipoles. The results from the artificial ferroelectric domains exclusively confirm the inherent coupling effect of IP and OOP ferroelectric polarization in 2D α -In₂Se₃.

To provide a proof-of-concept demonstration of the IP electric field control over the OOP electric polarization, we performed in situ PFM study on a planar device of α -In₂Se₃. Figure 2a shows the schematic of our two terminal device (optical image and the topography can be found in Figure S4, Supporting Information). Before applying the in-plane voltage, we balanced the upward and downward electric polarizations via artificial domain engineering, which could help to the better observation of the coupling effect in α -In₂Se₃. Here, we define the OOP polarization degree of the device with $P = \frac{D_{\downarrow} - D_{\uparrow}}{D_{\downarrow} + D_{\uparrow}}$, where D_{\downarrow} and D_{\uparrow} account the appearances of downward and upward electric polarization in the PFM measurements respectively. As shown in Figure 2b, a square downward artificial domain (bright area in the PFM phase image) is created with positive vertical PFM tip bias. Together with the spontaneous ferroelectric domains, the conducting channel of the device is divided into two oppositely polarized regions with almost equal size. Quantitatively, according to the statistics of D_{\downarrow} and D_{\uparrow} in Figure 2c, the P of the device at this initial state is negligible with the value of 5.2%. We then applied ± 40 V IP pulsed voltage, equivalent to an electric field at 4×10^4 V cm⁻¹ in this device, to flip the OOP electric polarizations. After applying +40 V IP bias pulse, the area of downward ferroelectric domain was suppressed (Figure 2d), suggesting the successful establishment of the upward electric polarization in the OOP direction. We found an increased P to 61.4% from the sharp contrast of D_{\downarrow} and D_{\uparrow} in Figure 2e. It should be highlighted that by -40 V IP voltage polarizing the device the domain pattern could be nearly restored to its fresh state with reduced P at 10.3% (Figure 2f–g). The reversible tuning on P via the planar bias validates the capability of the IP electric field control of the OOP electric polarization in α -In₂Se₃. Besides, we also observed clear OOP domain wall motion during the flipping process (Figure S5, Supporting Information), which was further evidence for this novel ferroelectricity control. It is worth nothing that, according to our previous PFM results, the switching electric field for the OOP ferroelectric polarization is at about 2×10^5 V cm⁻¹,^[22] which is much larger than the case in the IP direction.

Before constructing the CP-FET, we first quantify the gating ability of the OOP electric polarization in α -In₂Se₃. As studied earlier, due to the built-in electric field stemming from the electric polarization, large surface potential difference will be produced on the two sides of a given QL.^[26] Therefore, when integrated with other vdW material forming vertical heterojunction or device, the polarity of the ferroelectric layer determines its electronic structure and transport property through the electrostatic doping or the modulation on the interfacial Schottky barrier.^[22,23] However, it is challenge to measure such difference directly from the top and bottom surfaces of ultrathin vdW material in reality. Herein, as an indirect method, we perform study on opposite ferroelectric domains of α -In₂Se₃ with scanning Kelvin probe force microscopy (KPFM), which is sensitive to the distributions of surface electric potential and charges. Figure 3a sketches the band alignments with respect to the vacuum level for the top side of α -In₂Se₃ at its two degenerate polarized states. As visualized in Figure 3b,c, in a typical sample with spontaneous domains, we observed one to one correspondence of the surface potential mapping to the ferroelectric domain pattern. This correlation excludes the origin of

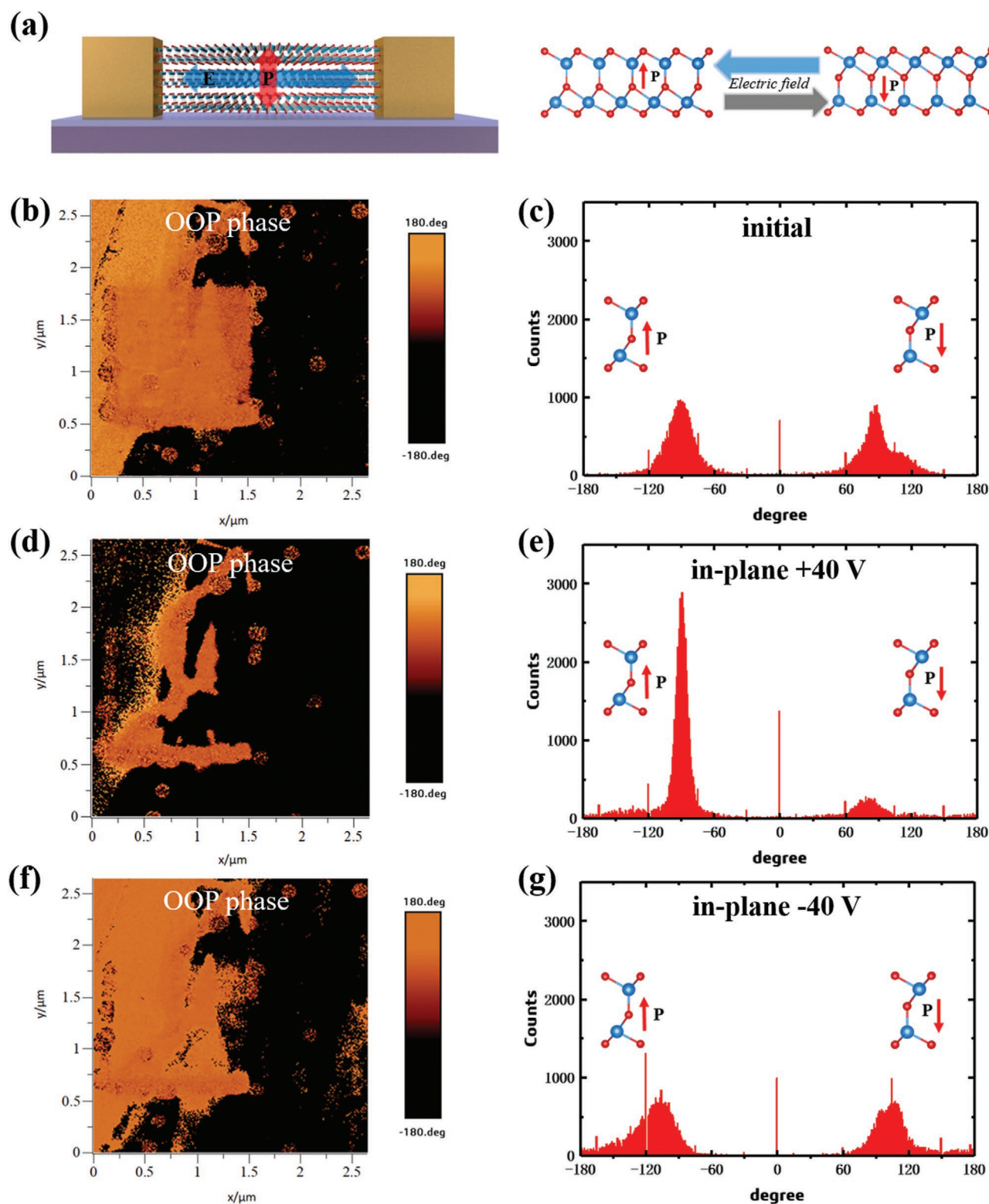


Figure 2. In-plane electric field control of the out-of-plane electric polarization. a) Schematic of the switching of OOP electric polarizations with IP electric field in a two-terminal device of ultrathin α - In_2Se_3 . b–g) In situ OOP electric polarization study with PFM. The OOP electric polarizations can be reversibly flipped by the IP bias of the proposed device in (a). The appearances of upward and downward electric polarizations in (b,d,f) are counted in (c,e,g) respectively.

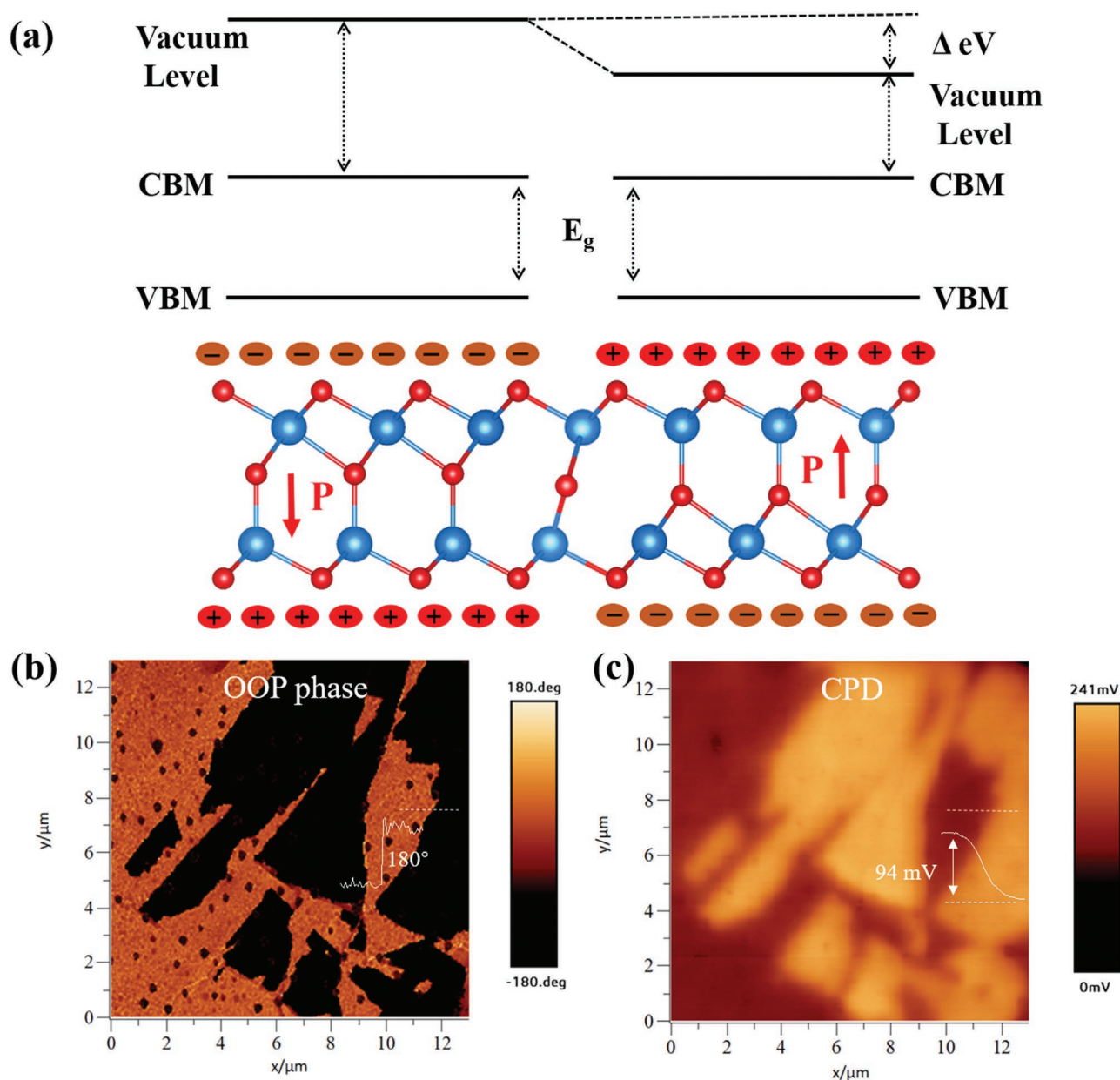


Figure 3. Surface potential of ferroelectric domains. a) The band alignments relative to vacuum level for downward and upward polarized α -In₂Se₃. The built-in electric field arising from the electric polarization leads to dramatic difference in surface potential. The positive and negative charges on the two sides of a QL stand for the polarization charges. b) Spontaneous OOP ferroelectric domains visualized by PFM. The phase profile of different ferroelectric domains is sketched by the dash line. A phase contrast of 180° is observed, which indicates the antiparallel directions of OOP polarization between the adjacent domains. c) The corresponding KPFM measurement on the ferroelectric domains in (b). The surface potential difference of antiparallel polarized OOP domains is found to be 94 mV.

the fluctuation in KPFM image from trapped charges or defects in α -In₂Se₃. Within each single domain, the contact potential signal is uniform. Between domains with antiparallel electric polarizations, the contact potential difference (CPD) were found to be 0.094 eV. At room temperature, under thermal equilibrium condition, the charge density within the same material follows $\Delta n = \exp(\frac{\Delta CPD}{k_b T})$, where Δn represents the carrier density ratio, k_b is the Boltzmann constant, and T is the temperature. Therefore, with $\Delta CPD = 0.094$ eV, the relative change of surface charge

density between upward and downward electrically polarized α -In₂Se₃ is as high as 10 times, which is able to induce significant electrostatic doping in vertical heterostructures.

The CP-FET was constructed via stacking 2H-MoS₂ (bottom) and α -In₂Se₃ (top) vertically into heterojunction. In the device, MoS₂ and α -In₂Se₃ formed a cross bar like structure and were used as conducting channel and gate dielectric respectively. Figure 4a,b shows the 3D schematic view and optical image of our CP-FET (device #1). The as-prepared device is with four

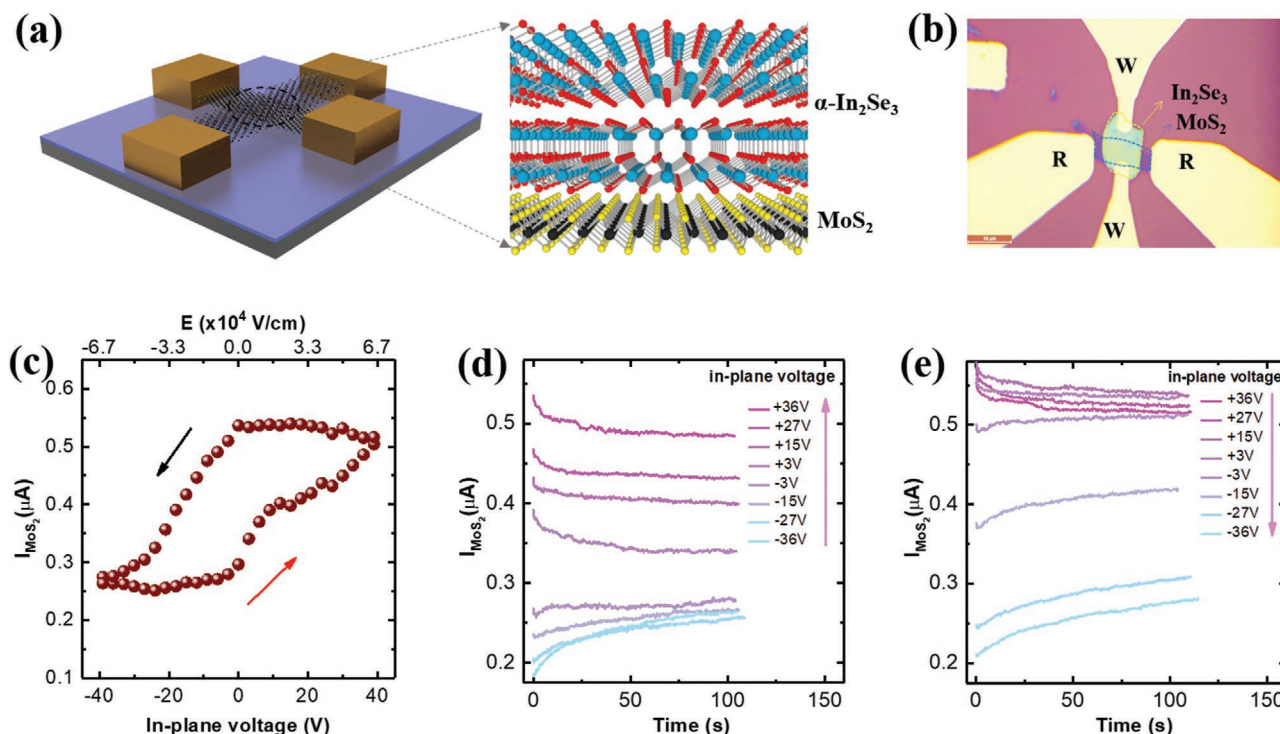


Figure 4. Demonstration of the in-plane voltage gated field-effect transistor. a) 3D schematic diagram of the CP-FET. The CP-FET is fabricated by vertically stacking MoS₂ and α -In₂Se₃ thin layers. The zoomed area shows the crystal structure of the MoS₂/ α -In₂Se₃ heterostructure. b) Optical image of the CP-FET device. c) The hysteretic in-plane ferromagnetic gating of the CP-FET. The conductance of the MoS₂ channel is tuned by the IP gate voltage with clear electrical hysteresis loop. d,e) Time dependent conductance study of the CP-FET. The variation of the channel current follows the decay of the electric polarizations. The arrow indicates the measuring sequence.

coplanar electrodes, among which two are used to read and the others are in charge of gating (or writing). The I - V characteristics of the CP-FET was measured by applying a relatively low voltage on the drain-source channel. The channel current (I_{MoS_2}) was linearly dependent on the bias (Figure S6, Supporting Information), indicating the Ohmic contacts between the metal electrode and MoS₂ few layers. To test the in-plane voltage gating effect in our CP-FET, we applied an transient IP voltage (V_{in}) on α -In₂Se₃ to control its OOP polarization which eventually induced the electrostatic doping in MoS₂, resulting the modulation on channel conductance. It should be noted that the MoS₂ channel was in open circuit when applying the IP polarizing voltage on α -In₂Se₃. This helped to exclude the establishment of OOP polarization from the vertical bias generated on α -In₂Se₃ and MoS₂. When measuring the I_{MoS_2} , similar operation was applied on the gating electrodes. In the transfer characteristic measurement of the CP-FET, as a transient gating, the IP polarization process on α -In₂Se₃ was kept for 10 s before measuring the I_{MoS_2} . After 100 s for the electric polarization to get stable, a constant bias was applied on MoS₂ to detect the channel current I_{MoS_2} . Figure 4c shows the I_{MoS_2} as the function of the IP gate voltage V_{in} . We observed clear hysteresis loop with conductance modulation as observed in previous 2D FeFETs.^[13] As the V_{in} was switched from -39 to $+39$ V back and forth, the I_{MoS_2} could be effectively tuned from 0.26 to 0.52 μA and vice versa with 200% change. This conductance variation is the result of the OOP electric polarization flipping by the IP

electric field, which stems from the inherent coupling of the IP and OOP polarizations in α -In₂Se₃.

To study the dynamical evolution of OOP electric polarizations under the control of the IP voltage, we measured the time dependent channel current I_{MoS_2} immediately after polarizing the α -In₂Se₃ with different V_{in} pulses as shown in Figure 4d,e. With negative IP voltage polarization, the conductance gradually increased to a stable state, while the I_{MoS_2} decreased after the initialization by positive IP voltage. Such different behaviors are well expected from the ferroelectric nature of α -In₂Se₃. For ferroelectrics, after the establishment of polarization, the ordering of electric dipoles will be disturbed by environmental thermal fluctuations and slowly decay to a stable state, resulting the so-called remnant electric polarization. Therefore, in the CP-FET, after the IP gate voltage polarizing, the conductance started to decay but with opposite directions for negative and positive bias. With a time span of 100 s, the device got to the constant conducting state. From the time dependent study, the CP-FET was found to be retentive, showing the nonvolatile functionality. We summarized more detailed time evolution of the conductance as well as the electrical hysteresis in Figures S7 and Figure S9 (Supporting Information).

For the further check on the validity of our CP-FET, we carried out two control experiments. First of all, since all the electrical measurements were carried out in vacuum, the possibility that surface charge traps induce the above current modulation and the electrical hysteresis loop can be excluded. The hysteretic

conduction modulation in the device was attributed to the screening effect of the electric polarizations of ferroelectrics. Therefore, artificially tuning the distance between the ferroelectric layer and the semiconductor can significantly affect the generation of screening charges. Here, we fabricated a gapped CP-FET (termed as device #2) with MoS₂/hBN/ α -In₂Se₃ vertical heterostructure as shown in Figure S8 (Supporting Information). Ultrathin hBN was used as buffer layer which increases the distance between the ferroelectric α -In₂Se₃ and MoS₂. Even in this type of gapped CP-FET, we observed the same electrical hysteresis but with relatively weak conductance modulation. It was well expected as a result of the imperfect screening of electric polarizations. Moreover, we made a device of MoS₂/MoS₂ homostructure to rule out the possible origin from electrostatically trapped charge or charge transfer between vdW layers (Figure S11, Supporting Information). With the same measuring sequence used in the study of CP-FET, the channel current in the bottom MoS₂ was found to be keeping constant when scanning the in-plane bias applied on the top MoS₂ layer. No electrical hysteresis was observed in this type of device.

In summary, we have presented a new approach to generate the electric field-effect with layered ferroelectric α -In₂Se₃ under room temperature. An in-plane voltage gated CP-FET with retentive switching effect have been demonstrated. This novel gating effect originates from the unique inter-locking of electric dipoles in α -In₂Se₃. It provides an unprecedented platform to develop novel functional nanoelectronic devices with vdW materials.

Experimental Section

Sample Preparation and Topography Measurements: Bulk single crystal graphite, 2H-MoS₂, hBN, and α -In₂Se₃ used in this study were purchased from 2D Semiconductors Inc. and Alfa Aesar Inc. respectively. Ultrathin vdW materials were prepared by the mechanical exfoliation onto Si substrate with 300 nm SiO₂ on top or transparent PDMS substrate (Gel-Pak, WF-60-X4) for stacking heterostructure. The topography and thickness of these ultra-thin samples were characterized by atomic force microscopy (AFM) (AIST-SmartSPM) at tapping mode.

Raman Spectroscopy Characterization: Raman spectra were taken with Horiba micro-Raman system (Labram HR Evolution). The wavelength of the laser excitation was 633 nm with on-sample power at around 100 μ W. For α -In₂Se₃, as shown in Figure S1 (Supporting Information), five characteristic Raman modes were observed to confirm its ferroelectric phase. For MoS₂ few layers, the E_{2g}¹ and A_{1g} phonon modes were used to identify their layer number.^[30] In the CP-FET (device #1), it is found that the peak locations of E_{2g}¹ and A_{1g} Raman modes of ultrathin MoS₂ were centered at 383.8 and 405.2 cm⁻¹ respectively with the wavenumber difference of 21.4 cm⁻¹ (Figure S6, Supporting Information), which confirmed the MoS₂ used in this device was bilayer.

PFM Measurements: PFM measurements were performed with the same AIST-SmartSPM by using gold coated conducting Si tip under ambient condition. The conductive substrates used in this study were prepared through sputtering 20 nm thick gold film onto Si substrate with 300 nm SiO₂ on top.

The CP-FET Device Fabrication and Transport Measurement: MoS₂ few layers were transferred onto SiO₂/Si⁺⁺ by micromechanical exfoliation. A suitable few layer α -In₂Se₃ was exfoliated from bulk material. This few layer α -In₂Se₃ was then accurately transferred on to the top of MoS₂ bilayer via the all-dry transfer technique.^[31] The cross bar like electrodes were fabricated by standard UV lithography and the following electron beam evaporation of 10 nm Ti and 70 nm Al. Keysight B2900 source

meter was used to measure the *I*-*V* and transfer characteristics of the devices. All the measurements were performed in a vacuum chamber under the pressure at 1×10^{-2} Pa.

Supporting Information

Supporting Information is available from the Wiley Online Library or from the author.

Acknowledgements

This work was supported by the National Key Research and Development Program of China (Grant Nos. 2017YFA0205004, 2018YFA0306600, and 2017YFA0204904), the National Natural Science Foundation of China (Grant Nos. 11674295, 11674299, 11374273, 11634011, and 51732010), the Fundamental Research Funds for the Central Universities (Grant Nos. WK2340000082, WK2030020032, and WK2060190084), Anhui Initiative in Quantum Information Technologies (Grant No. AHY170000), the Strategic Priority Research Program of Chinese Academy of Sciences (Grant No. XDB30000000), and the China Government Youth 1000-Plan Talent Program. This work was partially carried out at the USTC Center for Micro and Nanoscale Research and Fabrication.

Conflict of Interest

The authors declare no conflict of interest.

Author Contributions

Y.L. and C.C. contributed equally to this work. H.Z. and W.Z. conceived the idea and supervised the research. Y.L., X.M., W.L., and H.L. prepared the samples. A.N., J.X., and Z.L. contributed to the high-resolution atomic structure identification with AC-STEM. Y.L., C.C., and W.L. fabricated the devices, carried out the transport, PFM, and Raman spectrum measurements of the CP-FETs. Y.L., C.C., and H.Z. analyzed the data, wrote the paper, and all authors commented on the manuscript.

Keywords

2D ferroelectrics, 2D FETs, α -In₂Se₃

Received: January 14, 2020

Revised: May 8, 2020

Published online: June 11, 2020

- [1] C. H. Ahn, S. Gariglio, P. Paruch, T. Tybell, L. Antognazza, J.-M. Triscone, *Science* **1999**, 284, 1152.
- [2] C. H. Ahn, J. M. Triscone, J. Mannhart, *Nature* **2003**, 424, 1015.
- [3] J. T. Ye, Y. J. Zhang, R. Akashi, M. S. Bahramy, R. Arita, Y. Iwasa, *Science* **2012**, 338, 1193.
- [4] Y. Deng, Y. Yu, Y. Song, J. Zhang, N. Wang, Z. Sun, Y. Yi, Y. Wu, S. Wu, J. Zhu, J. Wang, X. Chen, Y. Zhang, *Nature* **2018**, 563, 94.
- [5] Y. Yu, F. Yang, X. Lu, Y. Yan, Y. Cho, L. Ma, X. Niu, S. Kim, Y.-W. Son, D. Feng, S. Li, S.-W. Cheong, X. Chen, Y. Zhang, *Nat. Nanotechnol.* **2015**, 10, 270.
- [6] Y. Wang, J. Xiao, H. Zhu, Y. Li, Y. Alsaïd, K. Fong, Y. Zhou, S. Wang, W. Shi, Y. Wang, A. Zettl, E. J. Reed, X. Zhang, *Nature* **2017**, 550, 487.

- [7] B. Lei, N. Z. Wang, C. Shang, F. B. Meng, L. K. Ma, X. G. Luo, T. Wu, Z. Sun, Y. Wang, Z. Jiang, B. H. Mao, Z. Liu, Y. J. Yu, Y. B. Zhang, X. H. Chen, *Phys. Rev. B* **2017**, 95, 020503.
- [8] L. Ju, Z. Shi, N. Nair, Y. Lv, C. Jin, J. Velasco Jr, C. Ojeda-Aristizabal, H. A. Bechtel, M. C. Martin, A. Zettl, J. Analytis, F. Wang, *Nature* **2015**, 520, 650.
- [9] J. Li, K. Wang, K. J. McFaul, Z. Zern, Y. Ren, K. Watanabe, T. Taniguchi, Z. Qiao, J. Zhu, *Nat. Nanotechnol.* **2016**, 11, 1060.
- [10] Y. Zhang, J. Ye, Y. Matsushashi, Y. Iwasa, *Nano Lett.* **2012**, 12, 1136.
- [11] S. Z. Bisri, S. Shimizu, M. Nakano, Y. Iwasa, *Adv. Mater.* **2017**, 29, 1607054.
- [12] S. Mathews, R. Ramesh, T. Venkatesan, J. Benedetto, *Science* **1997**, 276, 238.
- [13] M. Si, P. Liao, G. Qiu, Y. Duan, P. D. Ye, *ACS Nano* **2018**, 12, 6700.
- [14] K. S. Novoselov, A. K. Geim, S. V. Morozov, D. Jiang, Y. Zhang, S. V. Dubonos, I. V. Grigorieva, A. A. Firsov, *Science* **2004**, 306, 666.
- [15] K. Ueno, S. Nakamura, H. Shimotani, A. Ohtomo, N. Kimura, T. Nojima, H. Aoki, Y. Iwasa, M. Kawasaki, *Nat. Mater.* **2008**, 7, 855.
- [16] R. B. Jacobs-Gedrim, M. Shanmugam, N. Jain, C. A. Durcan, M. T. Murphy, T. M. Murray, R. J. Matyi, R. L. Moore, B. Yu, *ACS Nano* **2014**, 8, 514.
- [17] J. Zhou, Q. Zeng, D. Lv, L. Sun, L. Niu, W. Fu, F. Liu, Z. Shen, C. Jin, Z. Liu, *Nano Lett.* **2015**, 15, 6400.
- [18] X. Tao, Y. Gu, *Nano Lett.* **2013**, 13, 3501.
- [19] M. Si, A. K. Saha, S. Gao, G. Qiu, J. Qin, Y. Duan, J. Jian, C. Niu, H. Wang, W. Wu, S. K. Gupta, P. D. Ye, *Nat. Electron.* **2019**, 2, 580.
- [20] F. Xue, W. Hu, K.-C. Lee, L.-S. Lu, J. Zhang, H.-L. Tang, A. Han, W. Hsu, S. Tu, W. Chang, C.-H. Lien, J.-H. He, Z. Zhang, L. Li, X. Zhang, *Adv. Funct. Mater.* **2018**, 28, 1803738.
- [21] J. Xiao, H. Zhu, Y. Wang, W. Feng, Y. Hu, A. Dasgupta, Y. Han, Y. Wang, D. A. Muller, L. W. Martin, P. Hu, X. Zhang, *Phys. Rev. Lett.* **2018**, 120, 227601.
- [22] S. Wan, Y. Li, W. Li, X. Mao, W. Zhu, H. Zeng, *Nanoscale* **2018**, 10, 14885.
- [23] S. M. Poh, S. J. R. Tan, H. Wang, P. Song, I. H. Abidi, X. Zhao, J. Dan, J. Chen, Z. Luo, S. J. Pennycook, A. H. Castro Neto, K. Loh, *Nano Lett.* **2018**, 18, 6340.
- [24] C. Cui, W. Hu, X. Yan, C. Addiego, W. Gao, Y. Wang, Z. Wang, L. Li, Y. Cheng, P. Li, X. Zhang, H. N. Alshareef, T. Wu, W. Zhu, X. Pan, L. Li, *Nano Lett.* **2018**, 18, 1253.
- [25] Y. Zhou, D. Wu, Y. Zhu, Y. Cho, Q. He, X. Yang, K. Herrera, Z. Chu, Y. Han, M. C. Downer, H. Peng, K. J. Lai, *Nano Lett.* **2017**, 17, 5508.
- [26] W. Ding, J. Zhu, Z. Wang, Y. Gao, D. Xiao, Y. Gu, Z. Zhang, W. Zhu, *Nat. Commun.* **2017**, 8, 14956.
- [27] J. F. Scott, C. A. Paz de Araujo, *Science* **1989**, 246, 1400.
- [28] Z. Fei, W. Zhao, T. A. Palomaki, B. Sun, M. K. Miller, Z. Zhao, J. Yan, X. Xu, D. H. Cobden, *Nature* **2018**, 560, 336.
- [29] S. Wan, Y. Li, W. Li, X. Mao, C. Wang, C. Chen, J. Dong, A. M. Nie, J. Xiang, Z. Liu, W. Zhu, H. Zeng, *Adv. Funct. Mater.* **2019**, 29, 1808606.
- [30] C. Lee, H. Yan, L. E. Brus, T. F. Heinz, J. Hone, S. Ryu, *ACS Nano* **2010**, 4, 2695.
- [31] A. Castellanos-Gomez, M. Buscema, R. Molenaar, V. Singh, L. Janssen, H. S. J. van der Zant, G. A. Steele, *2D Mater.* **2014**, 1, 011002.